Spontaneously Gapped Ground State in Suspended Bilayer Graphene

F. Freitag,[1] J. Trbovic,[1] M. Weiss,[1] and C. Schönenberger[1,*]

[1]*Department of Physics, University of Basel, Klingelbergstrasse 82, CH-4056 Basel, Switzerland*

(Received 23 June 2011; published 13 February 2012)

Bilayer graphene bears an eightfold degeneracy due to spin, valley, and layer symmetry, allowing for a wealth of broken symmetry states induced by magnetic or electric fields, by strain, or even spontaneously by interaction. We study the electrical transport in clean current annealed suspended bilayer graphene. We find two kinds of devices. In bilayers of type $B1$ the eightfold zero-energy Landau level is partially lifted above a threshold field revealing an insulating $\nu = 0$ quantum-Hall state at the charge neutrality point. In bilayers of type $B2$ the Landau level lifting is full and a gap appears in the differential conductance even at zero magnetic field, suggesting an insulating spontaneously broken symmetry state. Unlike $B1$, the minimum conductance in $B2$ is not exponentially suppressed, but remains finite with a value $G \lesssim e^2/h$ even in a large magnetic field. We suggest that this phase of $B2$ is insulating in the bulk and bound by compressible edge states.

DOI: 10.1103/PhysRevLett.108.076602 PACS numbers: 72.80.Vp, 73.22.Pr, 73.23.−b, 73.43.Qt

Two-dimensional electron systems can host a large variety of ground states. Celebrated examples are the fractional quantum-Hall effect [1–3] and the Wigner crystal [4], both being driven by Coulomb interaction. Bilayer graphene provides a further class of interacting two-dimensional electron systems [5]. In contrast to single layer graphene, the chiral charge carriers are massive due to the coupling between the two layers [6,7]. Owing to the large number of symmetries, a wealth of ground states has been predicted [8–13]. This includes states in which a gap forms spontaneously in zero magnetic and electric fields, as opposed to the induced gap caused by the application of an external field [14–16] or mechanical strain [17,18]. Unlike a single layer, the interaction parameter r_s increases for low carrier concentrations n in bilayer graphene. To reach a low minimal n at the charge neutrality point (CNP), the effective disorder potential has to be sufficiently small. This can be achieved by current annealing [19] and by suspending the graphene sheet [20].

Bilayer graphene has an eightfold degenerate Landau level (LL) at zero energy. As the Hall conductivity is quantized at values of $\sigma_{xy} = \nu e^2/h$, where the filling factor ν is given by $\nu = \pm 4(N + 1)$, a step of 8 e^2/h is observed from $\nu = -4$ to $\nu = 4$ around the CNP [7]. A lifting of the spin symmetry, for example, manifests itself in the appearance of new Hall plateaus, of which $\nu = 0$ is the most prominent one [21]. If all symmetries are lifted, quantum-Hall plateaus appear at filling factors $\nu = 0, \pm 1, \pm 2, \pm 3, \ldots$. Magnetic fields of 30–45 T were required to see this lifting in SiO_2 supported devices, for both single [22] and bilayer graphene [23], until Feldman *et al.* succeeded in observing the effect at low-magnetic fields in suspended bilayer graphene [21].

The most striking state is the $\nu = 0$ state, whose nature is under debate for both single layer [24–26] and bilayer graphene [16,21,23]. For bilayer graphene, several possibilities are being discussed, such as the quantum-Hall ferromagnet [12,27,28], the quantum anomalous Hall insulator [11,29], or a ferroelectric phase [10].

We report on suspended and current annealed bilayer samples. We find two kinds of samples, $B1$ and $B2$, where $B2$ represents a new class. Differential conductance spectroscopy reveals that $B2$ samples are evidentially gapped at the CNP in zero magnetic and electric fields. Since $B2$ samples were annealed for an extended period we think that they are cleaner than $B1$ samples.

Suspended graphene devices were fabricated by mechanical exfoliation of natural graphite transferred to a doped Si wafer with a 300 nm top SiO_2 layer. The number of graphene layers was determined by Raman spectroscopy. The devices were then annealed for several hours in vacuum (10^{-7} mbar) at 200 °C before the electrical contacts made from Cr/Au (1/70 nm) were fabricated by electron-beam lithography. Thereafter, SiO_2 was etched in buffered hydrofluoric acid. After mounting a device into a ^{3}He cryostat, we performed current annealing by applying a dc current at 1.5 K. This procedure was repeated with higher current densities up to 500 μA/μm until the electrical conductance $G(V_g)$ showed a pronounced dependence as a function of the gate voltage V_g with a conductance minimum (CNP) close to $V_g = 0$, reminiscent of a high quality device. Conductance measurements were carried out with a lock-in amplifier applying a 20 μV ac voltage onto which a dc bias voltage could be superimposed.

Figure 1 shows representative measurements of the two-terminal conductance G of suspended graphene devices when n is altered by the back-gate voltage V_g. The CNP is close to $V_g = 0$ V for all samples, indicating that only a few charged impurities reside on the graphene. Both single layer and bilayers of type $B1$ display a smooth transition from low G at the CNP to higher G values at larger n, as expected from the V-shaped conductances found in recent literature [21,30,31]. In contrast, bilayer samples of type

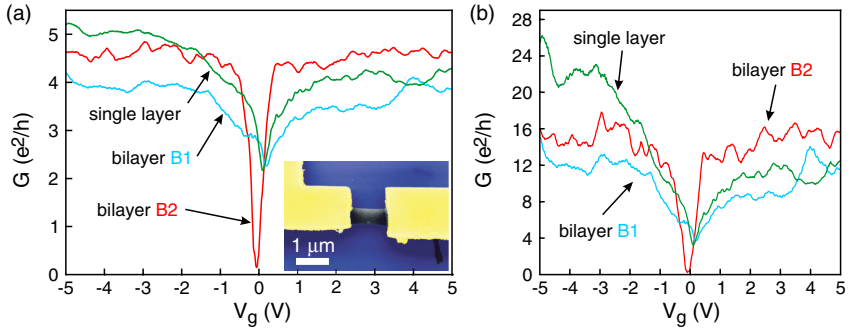

FIG. 1 (color online). (a) Comparison of the measured dependence of the conductance G on the applied gate voltage V_g for three suspended devices: single layer graphene (length × width 1×2 μm^2, $T = 2$ K), bilayer type $B1$ (2×0.8 μm^2, $T = 230$ mK), and bilayer type $B2$ (1×1.5 μm^2, $T = 230$ mK). In (b) the contact resistance was subtracted.

$B2$ are very low conducting at the CNP with $G_{\min} < 0.2$ e^2/h at 230 mK, which is considerably lower than in previous reports [16]. Furthermore, as the gate voltage is tuned away from the CNP, G increases sharply and then quickly saturates for $|V_g| > 0.5$ V. Note, that this is even the case when the contact resistance is subtracted as shown in Fig. 1(b).

When placed in a perpendicular magnetic field B, samples $B1$ and $B2$ reveal substantially different quantum-Hall features, as shown in Fig. 2. As the measurements were performed in a two-terminal configuration, they include a contact resistance [32]. We determined the contact resistance by matching G to the closest integer value of the quantized Hall conductance (Supplemental Material [33]) and then subtracted it from the data. First, we discuss sample $B1$ and then sample $B2$.

In sample $B1$, we observe a partial lifting of the eightfold zero-energy LL degeneracy, leading to the $\nu = \pm 2$ and 0 states above a critical magnetic field of $B_{\text{crit}} \approx 0.75$ T [Fig. 2(a)]. In the magnetic field range $0 \leq B \leq$

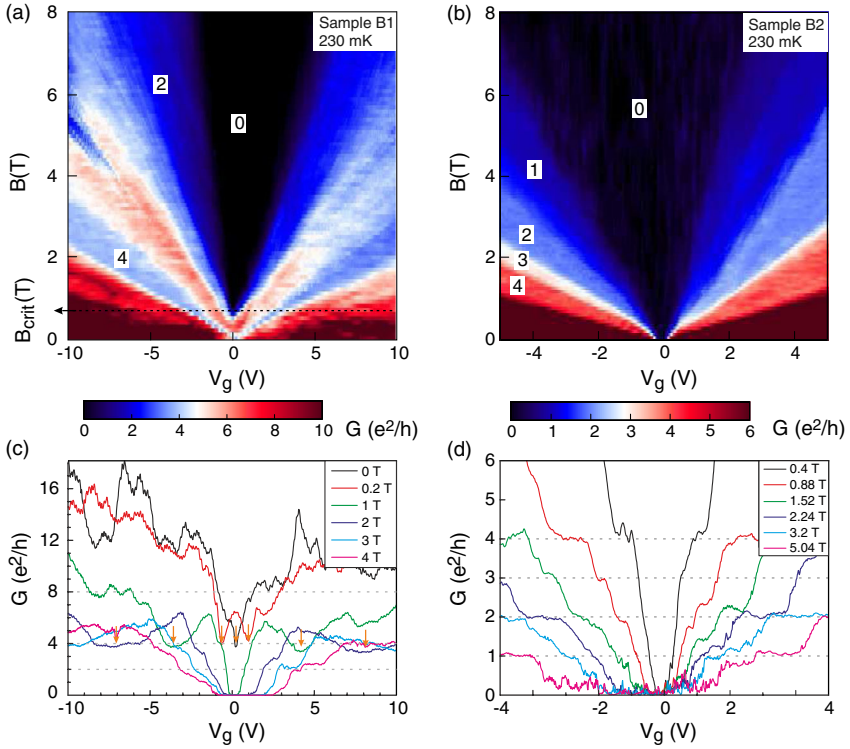

FIG. 2 (color online). The dependence of the linear conductance G on the gate voltage V_g and perpendicular magnetic field B reveals two types of samples. In sample $B1$, shown in (a), (c) the plateaus at filling factors $\nu = 0, \pm 2$, and ± 4 are well developed. The $\nu = \pm 4$ plateau [minima in (c), see arrows] extends to very low-magnetic fields. For sample $B2$, a full lifting of the eightfold Landau level degeneracy is observed, as plateaus at odd fillings appear as well. The curves in (c), (d) show line cuts at constant B. Appropriate contact resistances were subtracted.

0.75 T, we observe the same Hall sequence as in conventional devices where the conductance has a step of 8 e^2/h from $\nu = -4$ to $+4$. When applying $B > B_{crit}$ an insulating state emerges around the CNP, followed by the $\nu = \pm 2$ state with a twofold degeneracy remaining. We also note that the $\nu = \pm 4$ state appears to extend all the way down to the CNP at zero magnetic field [11,34]. The corresponding line cuts from the color scale are shown in Fig. 2(c) to illustrate the evolution of the CNP into the $\nu = \pm 4$ state at low fields and the appearance of the broken symmetry states $\nu = 0$ and ± 2 at higher fields [21]. Unlike sample $B1$, $B2$ shows a fully lifted zero-energy LL, manifesting in the appearance of Hall plateaus for odd filling factors ν. In analogy to sample $B1$, we label the low conducting region around the CNP in sample $B2$ with $\nu = 0$, although this state maintains a finite conductance as we will discuss below.

In the following Fig. 3, we investigate the properties of the low conducting state at $\nu = 0$ at low charge carrier density as a function of B and T for both samples. For device $B1$ [Fig. 3(a)], we find that at low B the resistance R at the CNP remains around $R = 6$ kΩ, but when a critical perpendicular magnetic field of $B_{crit} \approx 0.75$ T is reached, it increases sharply to 10^8 Ω, the maximum resistance that our measurement setup can resolve. This behavior can be attributed to the formation of a quantum-Hall state at $\nu = 0$ [25]. Since the Fermi energy now lies between two Landau levels, a thermally activated behavior is expected for the electrical resistance R. This is confirmed in the experiment, revealing a strong dependence of R on temperature T above the critical field following the law $R \propto \exp(\Delta E/2k_B T)$ [33]. The activation energy ΔE is linearly dependent on B with a value that amounts to 1.1 meV/T = 13 K/T. Note, that the spin Zeeman splitting is much smaller, only amounting to ~0.7 K/T. Feldman *et al.* [21] deduce in their experiment $\Delta E = 3.5 - 10.5$ K/T, which is somewhat lower than our number. In a recent theory, taking interactions into account, the energy gap of the $\nu = 0$ state has been calculated to be 14.3 K/T [12].

The dotted curves in Fig. 3(a) show the resistance R of $B2$ in direct comparison to that of $B1$ at 230 mK and 4 K. We find that at $B = 0$ T, $B2$ has an order of magnitude higher R than $B1$, whereas at higher magnetic fields, $B1$ is several orders more resistive. Figure 3(b) elaborates on the conductance of $B2$ at the CNP as a function of B and temperature. Most notably, G at $B \gtrsim 1$ T is nearly independent of B with the exception of fluctuations most likely caused by interference due to remaining localized states [3].

The marked differences in the magnetic field dependence clearly demonstrate that sample $B1$ and $B2$ differ. In sample $B1$, the LL degeneracy is partially lifted for $B > B_{crit} \approx 0.75$ T, revealing plateaus at $\nu = \pm 4$, $\nu = \pm 2$, and $\nu = 0$. On the other hand, sample $B2$ reveals a fully lifted LL, where all plateaus appear already at a small $B \sim 1$ T. Furthermore, sample $B2$ stays conductive at the CNP even at higher B of up to 8 T. We note, that sample $B1$ is similar in characteristics to the one reported by Feldman *et al.* [21], whereas $B2$ shows new features.

We further investigate the nature of sample $B2$ by measuring the differential conductance G_d as a function of the applied dc bias V_{sd} between source and drain contacts at $B = 0$ T at the CNP ($V_g = -0.1$ V), where G_d is suppressed. Figure 4(a) summarizes the findings for different temperatures from 226 mK to 4 K (no contact resistance subtracted). Two gaps can clearly be identified: When going from large source-drain bias $V_{sd} > 4$ mV towards small voltages, the larger gap Δ sets in at $V_{sd} = \pm 2.5$ mV, where G_d is decreased from around 4 e^2/h to 0.9 e^2/h in the data measured at 226 mK. The smaller gap δ appears at voltages $|V_{sd}| \lesssim 0.35$ mV and it reduces G_d from 0.9 e^2/h to less than 0.2 e^2/h. By increasing the temperature from

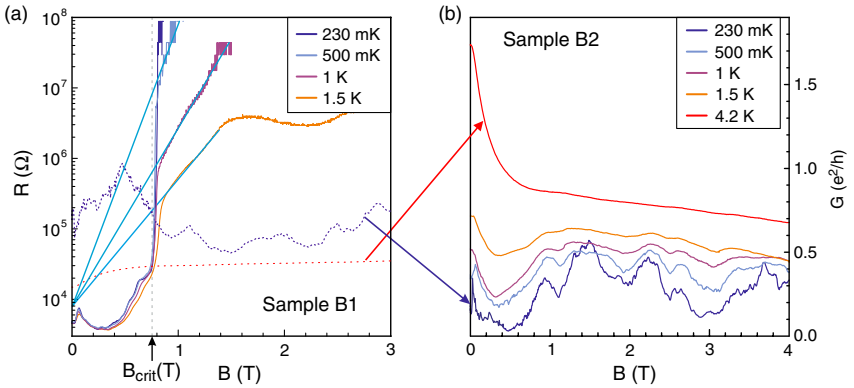

FIG. 3 (color online). Difference in resistance R (a) of sample $B1$ and conductance G (b) of sample $B2$ as a function of magnetic field B at the CNP. A sharp transition to an insulating $\nu = 0$ state appears at $B_{crit} = 0.75$ T (arrow) in $B1$. In this state, R is thermally activated [33] with an activation energy ΔE proportional to B. The lines are guides to the eyes for this dependence. For comparison, we show the resistance data for sample type $B2$ (dotted line) within the same graph. In contrast to sample $B1$, sample $B2$ does not show a field-induced transition to an insulating state. At low temperatures, G is remarkably insensitive to B, but displays a relatively low-conductance value $< e^2/h$. Appropriate contact resistances are subtracted.

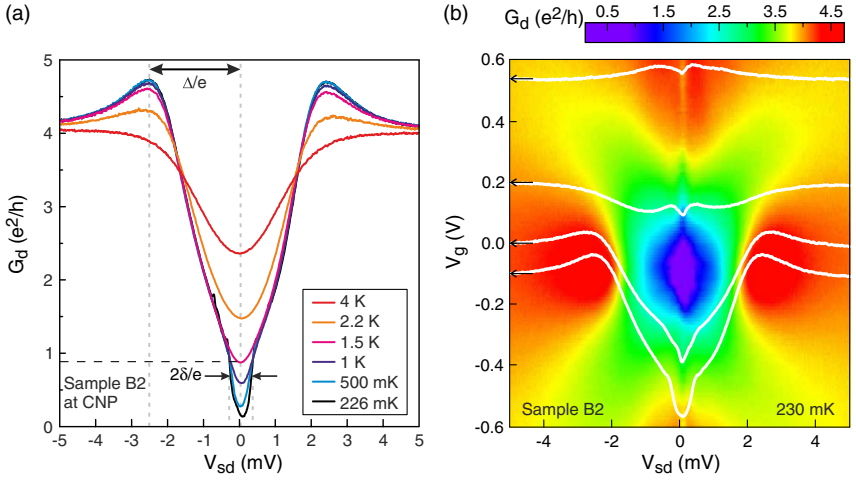

FIG. 4 (color online). (a) Temperature dependence of the differential conductance G_d around the CNP of sample $B2$ as a function of the source-drain bias voltage V_{sd}. Two gaps with size $\Delta = 2.5$ meV and $\delta = 0.35$ meV appear and both display a distinct temperature dependence. (b) Color-scale of G_d as a function of V_{sd} and gate voltage V_g at 230 mK. Line cuts are taken at the values of V_g marked by the arrows.

226 mK on, the smaller gap δ is first reduced and then vanishes at 1 K.

In order to identify the origin of these two gaps, a color-scale plot of the differential conductance G_d against V_{sd} and the gate voltage V_g at 230 mK is shown in Fig. 4(b). The line cut at the CNP ($V_g = -0.1$ V) shows again the two gaps in electron transport. As V_g and thus the charge carrier concentration is increased, the two gaps exhibit distinct changes. The larger gap Δ disappears, while the smaller gap δ still exists in the metallic graphene regime at $V_g > 0.5$ V, but with a less pronounced dip. This behavior is qualitatively consistent with Coulomb charging of the whole flake [35]. We estimate a single-electron charging energy of 1 meV for a flake of width 1.5 μm. Because the contact conductances of $\sim$4–8 e^2/h are substantially larger than e^2/h, charge quantization is only weak and no strong Coulomb blockade gap is expected. One rather expects the conductance to display a "weak" conductance suppression by something like 25–50% around zero bias, in agreement with the observation. In contrast to the small gap, the larger gap Δ is strongly dependent on the charge carrier density. At the CNP, it has its maximum magnitude, but only slightly away it starts to close. The line cut at $V_g = 0.2$ V already bears little sign of the gap Δ. Therefore, we conclude that it must be a feature intrinsic to the low-energy band structure of bilayer graphene and that this gap is formed spontaneously at zero magnetic and at *zero* electric field. We emphasize that the electric field due to the back-gate voltage in the vicinity of the gap feature is negligible. In the tight-binding band structure calculation of McCann [14], a gap of $\Delta = 2.5$ mV, as we observe it in our experiment, would require a back-gate voltage of at least 10 V.

The Δ gap can be associated with the $\nu = 0$ state, as the low-conductance region in the color-scale plot of Fig. 2(b) extends from large magnetic fields all the way down to zero magnetic field with no apparent phase boundary [33], distinctly different to the finding of Weitz *et al.* [16]. Although sample $B1$ and $B2$ have a $\nu = 0$ state around the CNP in our argument, these states are electrically different. In sample $B1$, the resistance evidently increases to infinity, whereas it stays finite in $B2$. This difference can be explained by insulating phases, differing in their edge-state structure [11,13,29].

Sample $B1$ has two phases, a low-magnetic field phase and a broken symmetry state induced by a small magnetic field of $B > B_{crit}$. The latter, most likely, is a quantum-Hall ferromagnet [11,12,27]. The phase at low-magnetic field has been assigned to a gapped anomalous Hall insulator in which topologically protected edge states should provide a conductance of up to 4 e^2/h [11,13,34]. This scenario is somewhat supported by the quantum-Hall states at $\nu = \pm 4$ that persist all the way down to $B = 0$ [see arrows in Fig. 2(c)]. A similar observation has been made in compressibility measurements by Martin *et al.* [34]. Because $B2$ is the cleaner sample of the two [36], we rather think that the low-field phase of $B1$ is a normal state, not a broken symmetry state. In contrast, the low-density phase of $B2$ is a broken symmetry state. To explain the finite conductance we propose edge states in the $B2$ phase. If we subtract the small gap δ in sample $B2$, the measured conductance G is ≈ 0.8 e^2/h, which is smaller than the ballistic channel conductance of any gapped phase with edge states. This suggests that the gapped phase is either not single domain or that the edge states are not topologically protected, allowing for partial backscattering. Further work is needed to determine the nature of the edge states and assign it to broken electron-hole, valley, or spin symmetry [11,13,37,38].

In conclusion, using differential conductance spectroscopy we found a new type of bilayer whose spectral density

is gapped at zero magnetic and zero electric fields. Though this state is due to an insulating phase, the nonvanishing conductance $\approx 0.8\ e^2/h$, which is surprisingly robust in magnetic field, suggests that edge states are present.

This work was financed by the Swiss NSF, the ESF programme Eurographene, the NCCR Nano and QSIT. We acknowledge access to Raman microscope provided by C. Stampfer and C. Hierold. We are also grateful to A. Baumgartner, V. I. Fal'ko, L. Levitov, D. Maslov, R. Maurand, A. Morpurgo, and A. Yacoby for discussions.

Note added.—In the course of the reviewing process of this paper, we became aware of an independent work, in which dI/dV spectroscopy is applied to clean bilayer graphene samples, revealing gaps [39].

*Electronic address: Christian.Schoenenberger@unibas.ch

[1] D. C. Tsui, H. L. Stormer, and A. C. Gossard, Phys. Rev. Lett. **48**, 1559 (1982).
[2] X. Du, I. Skachko, F. Duerr, A. Luican, and E. Y. Andrei, Nature (London) **462**, 192 (2009).
[3] K. I. Bolotin, F. Ghahari, M. D. Shulman, H. L. Stormer, and P. Kim, Nature (London) **462**, 196 (2009).
[4] E. Wigner, Phys. Rev. **46**, 1002 (1934).
[5] S. Das Sarma, S. Adam, E. H. Hwang, and E. Rossi, Rev. Mod. Phys. **83**, 407 (2011).
[6] E. McCann and V. I. Fal'ko, Phys. Rev. Lett. **96**, 086805 (2006).
[7] K. S. Novoselov, E. McCann, S. V. Morozovi, V. I. Fal'ko, M. I. Katsnelson, U. Zettler, D. Jiang, F. Schnedin, and A. K. Geim, Nature Phys. **2**, 177 (2006).
[8] H. Min, G. Borghi, M. Polini, and A. H. MacDonald, Phys. Rev. B **77**, 041407(R) (2008).
[9] R. Nandkishore and L. Levitov, Phys. Rev. Lett. **104**, 156803 (2010).
[10] F. Zhang, H. Min, M. Polini, and A. H. MacDonald, Phys. Rev. B **81**, 041402 (2010).
[11] R. Nandkishore and L. Levitov, Phys. Rev. B **82**, 115124 (2010).
[12] E. V. Gorbar, V. P. Gusynin, and V. A. Miransky, JETP Lett. **91**, 314 (2010).
[13] F. Zhang, J. Jung, G. A. Fiete, Q. Niu, and A. H. MacDonald, Phys. Rev. Lett. **106**, 156801 (2011).
[14] E. McCann, Phys. Rev. B **74**, 161403(R) (2006).
[15] J. B. Oostinga, H. B. Heersche, X. Liu, A. F. Morpurgo, and L. M. K. Vandersypen, Nature Mater. **7**, 151 (2007).
[16] R. T. Weitz, M. T. Allen, B. E. Feldman, J. Martin, and A. Yacoby, Science **330**, 812 (2010).
[17] S.-M. Choi, S.-H. Jhi, and Y.-W. Son, Nano Lett. **10**, 3486 (2010).
[18] M. Mucha-Kruczynski, I. L. Aleiner, and V. I. Fal'ko, Phys. Rev. B **84**, 041404 (2011).
[19] J. Moser, A. Barreiro, and A. Bachtold, Appl. Phys. Lett. **91**, 163513 (2007).
[20] K. Bolotin, K. J. Sikes, Z. Jiang, M. Klima, G. Fudenberg, J. Hone, P. Kim, and H. L. Stormer, Solid State Commun. **146**, 351 (2008).
[21] B. E. Feldman, J. Martin, and A. Yacoby, Nature Phys. **5**, 889 (2009).
[22] Y. Zhang, Z. Jiang, J. P. Small, M. S. Purewal, Y.-W. Tan, M. Fazlollahi, J. D. Chudow, J. A. Jaszczak, H. L. Stormer, and P. Kim, Phys. Rev. Lett. **96**, 136806 (2006).
[23] Y. Zhao, P. Cadden-Zimansky, Z. Jiang, and P. Kim, Phys. Rev. Lett. **104**, 066801 (2010).
[24] D. A. Abanin, K. S. Novoselov, U. Zeitler, P. A. Lee, A. K. Geim, and L. S. Levitov, Phys. Rev. Lett. **98**, 196806 (2007).
[25] J. G. Checkelsky, L. Li, and N. P. Ong, Phys. Rev. B **79**, 115434 (2009).
[26] L. Zhang, Y. Zhang, M. Khodas, T. Valla, and I. A. Zaliznyak, Phys. Rev. Lett. **105**, 046804 (2010).
[27] K. Nomura and A. H. MacDonald, Phys. Rev. Lett. **96**, 256602 (2006).
[28] M. Kharitonov, arXiv:1105.5386v1.
[29] S. Raghu, X.-L. Qi, C. Honerkamp, and S.-C. Zhang, Phys. Rev. Lett. **100**, 156401 (2008).
[30] S. V. Morozov, K. S. Novoselov, M. I. Katsnelson, F. Schedin, D. C. Elias, J. A. Jaszczak, and A. K. Geim, Phys. Rev. Lett. **100**, 016602 (2008).
[31] X. Du, I. Skachko, A. Barker, and E. Y. Andrei, Nature Nanotech. **3**, 491 (2008).
[32] J. R. Williams, D. A. Abanin, L. DiCarlo, L. S. Levitov, and C. M. Marcus, Phys. Rev. B **80**, 045408 (2009).
[33] See Supplemental Material at http://link.aps.org/supplemental/10.1103/PhysRevLett.108.076602 for device characterizations, additional B2 samples, and thermal cycling.
[34] J. Martin, B. E. Feldman, R. T. Weitz, M. T. Allen, and A. Yacoby, Phys. Rev. Lett. **105**, 256806 (2010).
[35] M. H. Devoret, D. Esteve, H. Grabert, G. L. Ingold, H. Pothier, and C. Urbina, Phys. Rev. Lett. **64**, 1824 (1990).
[36] We can convert $B2$ into $B1$ by exposing the sample to air. To convert $B1$ into $B2$ requires further current annealing at low temperatures.
[37] D. A. Abanin, P. A. Lee, and L. S. Levitov, Phys. Rev. Lett. **96**, 176803 (2006).
[38] I. Martin, Y. M. Blanter, and A. F. Morpurgo, Phys. Rev. Lett. **100**, 036804 (2008).
[39] J. Velasco Jr. *et al.*, Nature Nanotech. (in press).